Direct Imaging of Biological Sulfur Dioxide Derivatives in Vivo Using a Two-Photon Phosphorescent Probe

Li, Guanying ; Chen, Yu ; Wang, Jinquan ; Wu, Jingheng ; Gasser, Gilles ; Ji, Liangnian ; Chao, Hui

DOI: https://doi.org/10.1016/j.biomaterials.2015.06.014

Submitted to Biomaterials

Direct imaging of biological sulfur dioxide derivatives *in vivo* using a two-photon phosphorescent probe

Guanying Li,[1] Yu Chen,[1] Jinquan Wang,[1] Jingheng Wu,[1]

Gilles Gasser,[2] Liangnian Ji,[1] Hui Chao[1]*

[1]MOE Laboratory of Bioinorganic and Synthetic Chemistry, School of Chemistry and Chemical Engineering, Sun Yat-Sen University, Guangzhou 510275, P. R. China

[2] Department of Chemistry, University of Zurich, Winterthurestrasse 190, CH-8057 Zurich, Switzerland.

*Corresponding authors. Tel: 86-20-84112245; E-mail: ceschh@mail.sysu.edu.cn

ABSTRACT

Sulfur dioxide (SO_2) and its derivatives sulfite and bisulfite play important roles in biological systems. However, *in vivo* detection of sulfite/bisulfite remains challenging. In this study, we developed a dinuclear Ir(III) complex (**Ir4**) as a two-photon phosphorescent probe for sulfite and bisulfite. **Ir4** selectively and rapidly responded, with high sensitivity, to sulfite/bisulfite over other bio-related ions and molecules. One-photon and two-photon microscopy images revealed that **Ir4** preferentially targeted mitochondria and was capable of imaging biological sulfite/bisulfite levels *in vitro* and *in vivo*. *In situ* sulfite generation in *C. elegans* was visualized by two-photon excitation real-time imaging. Finally, **Ir4** was employed to monitor sulfite distribution in rat brain and other tissues. This study is the first report of the direct visualization of SO_2 derivatives *in vivo*. These results provide new insights into the biological importance of SO_2.

Keywords: Biological SO_2; Iridium(III) complex; Two-photon probe; *C. elegans*; Mice tissues

1. Introduction

In addition to its toxicity as an air pollutant, sulfur dioxide (SO_2) produces biological effects at physiological concentrations. Gaseous SO_2 has a short half-life of 1-2 seconds and dissociates into its sulfite/bisulfite (3:1) derivatives in plasma. Total sulfite content in serum is maintained at low levels (0-10 μM) [1]. Endogenous sulfite is enzymatically generated *via L*-cysteine catabolism [2]. More precisely, the key enzyme in the generation of sulfite is aspartate aminotransferase (AAT), which is constitutively expressed in the cytosol and mitochondria [3]. Of note, neutrophils also produce sulfite in response to endotoxins or oxidative stress [4,5]. Endogenous SO_2 and its derivatives appear

to be involved in various physiological processes, including vasorelaxation, anti-hypertensive effect, inhibition of vascular smooth muscle, and regulation of cardiac channel function. To some extent, the effect of SO_2 is similar to that of other gasotransmitters such as NO, CO and H_2S. For this reason, endogenous SO_2 has been recently recognized as a novel potential gasotransmitter [6-10]. However, this role remains controversial since the biological effects of sulfite are poorly understood and since SO_2 and its derivatives cannot be directly detected *in vivo*. The most commonly used method for the determination of sulfite/bisulfite in biological samples, namely high-performance liquid chromatographic (HPLC) [1], requires complex and invasive sample treatment and is not suitable for real-time and long-term detection of biological sulfite/bisulfite. Therefore, the development of a rapid, facile and reliable real-time detection method for biological sulfite/bisulfite levels is highly required.

Fluorescent imaging is one of the most attractive molecular imaging techniques for *in vivo* detection of biomolecules [11-14]. Hence, fluorescent probes for sulfite and/or bisulfite have been reported [15-18] and used for imaging of intracellular sulfite/bisulfite levels [19-21]. However, to the best of our knowledge, no probes for the determination of sulfite distribution in subcellular organelles are available. In addition, the reported probes for imaging of intracellular sulfite/bisulfite levels have been evaluated using one-photon microscopy (OPM) with relatively short excitation wavelengths. Two-photon microscopy (TPM) is becoming a powerful tool in molecular imaging of cells and tissues [22-26]. The advantages of two-photon excitation include reduced out-of-focus photobleaching, reduced autofluorescence, non-invasive excitation, deeper tissue penetration and intrinsically high three-dimensional resolution. This method would be particularly meaningful and valuable in monitoring sulfite/ bisulfite levels.

With this in mind, we aimed to develop a selective two-photon fluorescent probe for imaging biological sulfite/bisulfite *in vivo*. We previously developed

an Off-On phosphorescent probe (**Ir1**, Figure 1) for biological sulfite and bisulfite with one-photon excitation [27]. Probe **Ir1** has a moderate two-photon absorption (TPA) cross-section value (σ = 51.3 GM) but a relatively low phosphorescent quantum yield (ϕ = 0.081), resulting in low two-photon brightness or two-photon excitation action cross-section ($\sigma' = \sigma \times \phi$). In practice, a more relevant feature of a luminophore for use in TPM is its two-photon brightness σ' [24]. Higher values of σ' enable detection of lower probe concentrations at reduced laser powers, suppress autofluorescence, reduce phototoxic effects on the sample and facilitate higher resolution images of living cells and deep tissues. Many practical two-photon fluorescent dyes exhibit σ' values larger than 10 [22-26]. To achieve such values, a high luminescent efficiency and/or large TPA cross-section value is essential. Recently, the Cho's and Kim's groups have reported some benzothiazole and benzimidazole-based compounds that have strong two-photon emission [28-29]. With this in mind, we vary the auxiliary ligand of **Ir1** to tune the electronic and spectral properties of the Ir-azo complex system. Hence, a series of azo-based Ir(III) complexes $[Ir(C^N)_2(azobpy)Ir(C^N)_2]^{2+}$ (**azobpy** = 4,4''-azo-bis(2,2'-bipyridine)) with different cyclometalated ligands (C^N) were synthesized, and their spectral properties, sulfite sensing behaviors and cellular toxicities were compared in detail to identify an appropriate two-photon phosphorescent probe. The synthetic probes that were strongly emissive before reacting with sulfite or weakly emissive after reacting with sulfite were discarded. Three probes (**Ir2-Ir4**, Figure 1a) have passed this initial screening and are discussed in-depth in this paper.

2. Materials and methods

2.1. General instruments

Microanalysis (C, H, and N) was carried out using an Elementar Vario EL

elemental analyzer. Electrospray mass spectra were recorded on a LCQ system (Finnigan MAT, USA). Melting points were recorded on a WRS-1B digital melting point apparatus (Shanghai Precision Inst. Co., Ltd). ^{1}H NMR spectra were recorded on a 400 MHz Nuclear Magnetic Resonance Spectrometry (Varian, Mercury-Plus 400). All chemical shifts are reported relative to tetramethylsilane (TMS). ^{13}C NMR spectra were recorded on a 126 MHz Superconducting Fourier Transfer Nuclear Magnetic Resonance Spectrometry (Varian, INOVA500NB). All chemical shifts are reported relative to the solvent CD_3OD (δ = 48.8 ppm). Electronic absorption spectra were recorded using a Perkin-Elmer Lambda 850 UV/Vis Spectrometer. Emission spectra were recorded on a Perkin-Elmer LS 55 Luminescence Spectrometer. pH measurements were conducted with a Sartorius PB-10 pH-meter.

2.2. Materials and reagents

All purchased chemicals were used as received. Solvents were dried and distilled prior to synthesis. $IrCl_3$, benzaldehyde, benzene-1,2-diamine, 2-aminophenol, 2-aminobenzenethiol, 3-(4,5-dimethylthiazol-2-yl)-2,5-diphenyltetrazoliu bromide (MTT) were purchased from Alfa Aesar and were used without further purification. Commercially available mitochondrial imaging agents, Mito-tracker® Red FM (MTR) was purchased from Invitrogen. The ligands 2-phenyl-1H-benzo[d]imidazole (**pbi**) [30], 2-phenylbenzo[d]oxazole (**pbo**) [31], 2-phenylbenzo[d] thiazole (**pbt**) [31], and 4,4''-azobis(2-2'-bipyridine) (**azobpy**) [32] were synthesized according to literature methods.

*2.3. Synthesis of iridium(III) complexes (**Ir2~Ir4**)*

The cyclometalated iridium(III) chloro-bridged dimers were synthesized according to a procedure described in the literature [30,32] by refluxing $IrCl_3 \cdot 3H_2O$ with the corresponding cyclometalated ligands in a mixture of

2-ethoxythanol and water for 24 h. The crude products were precipitated, collected and used without further purification.

The synthesis of the cationic Ir(III) complexes was readily achieved from the reaction of cyclometalated chloride-bridged dimers with the corresponding ancillary ligands by a bridge-splitting reaction. In a general procedure, 0.1 mmol Ir(III) dimer and 0.1 mmol **azobpy** was placed in a 50 mL three-necked flask with 20 mL of methanol and trichloromethane (1:1, v/v). The mixture was heated to 65 ºC for 6 h under argon. Then solvent was evaporated under reduced pressure, and the crude product was purified by column chromatography on silica with CH_2Cl_2-MeOH (20:1, v/v) as the eluent. The obtained compound was then recrystallized with a mixture of CH_2Cl_2/hexane to obtain the iridium complexes.

Ir2: Yield 72.4 mg, 46%. Anal. Calc. for $C_{72}H_{50}N_{14}Cl_2Ir_2$ (%): C, 55.20; H, 3.22; N, 12.52. Found(%): C, 55.32; H, 3.14; N, 12.39. ESI-MS (CH_3OH): *m/z* 748.61 $[M\text{-}2Cl^-]^{2+}$. m.p. > 300 ºC. ^{1}H NMR (400 MHz, CD_3CN) δ 11.66 (s, 4H), 8.96 (dd, *J* = 7.2, 1.2 Hz, 2H), 8.64 (d, *J* = 8.0 Hz, 2H), 8.54 (d, *J* =6.0 Hz, 2H), 8.29 (d, *J* = 4.8 Hz, 2H), 8.21 (t, *J* = 8.0 Hz, 2H), 7.92 (dd, *J* = 6.0, 2.0 Hz, 2H), 7.81 (d, *J* = 7.2 Hz, 4H), 7.67 - 7.53 (m, 8H), 7.26 (t, *J* = 7.2 Hz, 4H), 7.11 (t, *J* = 7.6 Hz, 4H), 7.01 - 6.82 (m, 7H), 6.39 (dd, *J* = 14.8, 7.6 Hz, 3H), 6.01 - 5.89 (m, 2H), 5.77 (d, *J* = 8.4 Hz, 2H). ^{13}C NMR (126 MHz, CD_3OD) δ 175.0, 164.5, 159.5, 157.4, 156.6, 153.1, 151.5, 149.7, 139.5, 134.1, 133.5, 133.0, 130.3, 128.2, 124.3, 123.7, 123.3, 122.3, 119.9, 117.5, 113.0, 112.4.

Ir3: Yield 118.1 mg, 75%. Anal. Calc. for $C_{72}H_{46}N_{10}O_4Cl_2Ir_2$ (%): C, 55.06; H, 2.95; N, 8.92. Found(%): C, 55.12; H, 2.84; N, 8.89. ESI-MS (CH_3OH): *m/z* 749.91 $[M\text{-}2Cl^-]^{2+}$. m.p. > 300 ºC. ^{1}H NMR (400 MHz, CD_3CN) δ 9.32 (s, 1H), 8.98 (d, *J* = 8.4 Hz, 1H), 8.60 (t, *J* = 6.8 Hz, 2H), 8.36 (d, *J* = 6.8 Hz, 2H), 8.28 (d, *J* = 4.8 Hz, 2H), 8.22 - 8.12 (m, 2H), 8.02 (s, 2H), 7.95 (d, *J* = 7.6 Hz, 2H), 7.88 (d, *J* = 4.8 Hz,2H), 7.83 - 7.79 (m, 4H), 7.68 - 7.60 (m, 2H), 7.46 (dd, *J* = 16.4, 8.1 Hz, 4H), 7.22 - 7.11 (m, 8H), 7.03 (t, *J* = 6.4 Hz, 4H), 6.66 - 6.56 (m, 4H), 6.06 (t, *J* = 8.0 Hz, 2H), 5.83 (dd, *J* = 14.8, 7.6 Hz, 2H). ^{13}C NMR (126

MHz, CD_3OD) δ 182.3, 158.6, 158.1, 155.6, 152.2, 150.7, 149.6, 144.3, 140.3, 139.4, 134.3, 131.5, 130.8, 130.4, 129.5, 126.2, 125.6, 124.5, 123.9, 122.9, 120.6, 119.0.

Ir4: Yield 112.7 mg, 70%. Anal. Calc. for $C_{72}H_{46}N_{10}S_4Cl_2Ir_2$ (%): C, 52.90; H, 2.84; N, 8.57. Found(%): C, 52.82; H, 2.94; N, 8.69. ESI-MS (CH_3OH): *m/z* 782.51 $[M\text{-}2Cl^-]^{2+}$. m.p. > 300 °C. ^1H NMR (400 MHz, CD_3CN) δ 9.23 (dd, *J* = 4.8, 1.6 Hz, 2H), 8.94 - 8.85 (m, 2H), 8.41 (d, *J* = 6.0 Hz, 2H), 8.23 (t, *J* = 8.0 Hz, 2H), 8.19 (dd, *J* = 5.6, 1.2 Hz, 2H), 8.08 - 8.01 (m, 4H), 7.98 (dd, *J* = 7.6, 0.8 Hz, 4H), 7.95 (dt, *J* = 6.0, 2.0 Hz, 2H), 7.66 (dd, *J* = 7.2, 6.0 Hz, 2H), 7.43 - 7.34 (m, 4H), 7.19 - 7.11 (m, 8H), 6.95 (td, *J* = 8.8, 1.2 Hz, 4H), 6.43 (dd, *J* = 18.4, 7.6 Hz, 4H), 6.39 (d, *J* = 8.4 Hz, 2H), 6.22 (dd, *J* = 8.4, 2.0 Hz, 2H). ^{13}C NMR (126 MHz, CD_3OD) δ 180.8, 152.3, 150.9, 149.7, 149.4, 140.6, 140.1, 139.4, 133.8, 133.3, 132.0, 131.8, 131.5, 130.9, 128.9, 128.0, 126.8, 126.5, 125.8, 123.3, 122.8, 118.7, 117.8.

2.4. Phosphorometric analysis

Stock solution of **Ir2**-**Ir4** (1 mM) were prepared in DMSO and diluted to appropriate concentration with a PBS buffer before use. The appropriate analytes were then added. Both absorption spectra and emission spectra were measured after stirring for 5 min in standard 1.0 cm quartz cells. The mixture was equilibrated for 5 min before measurement. Excitation wavelength was 405 nm and both slits were set to 10 nm in the emission spectra.

2.5. Photophysical properties

The emission quantum yields of **Ir1**-**Ir4** in the absence or presence of sulfite were measured in PBS buffer containing 2% DMSO using $[Ru(bpy)_3]^{2+}$ as a standard [33]. The quantum yields were calculated according to eq. 1:

$$\phi_u = \phi_s \frac{I_u A_s}{I_s A_u} \quad (1)$$

where, I is the integrated fluorescent intensity, A is the integrated absorbance intensity. Subscript 'u' stands for reference samples, 's' stands for samples.

The TPA cross-section values of probes **Ir1**-**Ir4** were obtained by two-photon excitation fluorescence [34] using an OpeletteTM 355II (pulse width < 100 fs, 80 MHz repetition rate, tuning range 700-1050 nm, spectra Physics Inc., USA). Two-photon excited emission spectra were measured in fluorometric quartz cuvettes in CH_3OH at 298 K. The experimental luminescence excitation and detection conditions were conducted with negligible reabsorption processes, which can affect TPA measurements. The quadratic dependence of two-photon induced phosphorescent intensity on the excitation power was verified at an excitation wavelength of 750 nm. The TPA cross-section of the probe was calculated at each wavelength according to eq. (2)

$$\sigma_2 = \sigma_1 \frac{\phi_1 c_1 I_2 n_2}{\phi_2 c_2 I_1 n_1} \tag{2}$$

Among them, I is the integrated fluorescence intensity, c is the concentration, n is the refractive index, and ϕ is the quantum yield. Subscript '1' stands for reference, '2' stands for sample. In our measurements, we have ensured that the excitation flux and the excitation wavelengths are the same for both the sample and the reference. The two-photon absorption cross-sections δ of iridium complexes were determined using rhodamine B as a reference [35].

2.6. One- and two-photon cellular imaging

The HepG2 cells were seeded at a density of 2×10^6 cells per mL in DMEM medium, supplemented with 10% fetal bovine serum (Corning Inc.), 1% penicillin (Gibco), and 1% streptomycin (Gibco) at 37 °C in a 5% CO_2/95% air incubator. After 1 day, cells were treated without or with 20 μM Na_2SO_3 in DMEM media for 4 h. After removing the DMEM media and washing with PBS buffer three times, the cells were further incubated with 2.0 μM of **Ir4**

solutions in PBS containing 1% DMSO for 15 min and incubated with Mito Tracker Red for another 15 min. For endogenous sulfite detection, HepG2 cells were pre-treated with 500 μM/250 μM thiosulfate sulfurtransferase (TST) substrates $Na_2S_2O_3$/NaCN or $Na_2S_2O_3$/GSH overnight to increase sulfite/ bisulfite levels and then treated with **Ir4** for 30 min. In contrast experiments, 100 mM 2,4,6-trinitrobenesulfonate (TNBS) solution was added and then incubated for 2 h to inhibit TST activity. RAW 264.7 cells were pre-treated with 1 μg/mL LPS for 2 h, and allowed to incubate with 100 μM Na_2SO_4 solution in PBS for another 4 h to promote sulfite generation. In contrast experiment, prednisolone (0.1 μM) treated with cells for 4 h before LPS treatment to suppress the sulfite generation. After washing out the supplemented LPS, Na_2SO_4 or prednisolone, RAW264.7 cells were further incubated with **Ir4** (2.0 μM, 30 min). The cells were washed three times carefully with PBS buffer and then subjected to luminescence imaging measurements. Cell images were captured with a monochromatic Cool SNAP FX camera (Roper Scientific, USA) and analyzed by using Axio Vision 4.2 software (Carl Zeiss).

2.7. Two-photon imaging of C. elegans

C. elegans was cultured as previously described [36] and maintained at 20 °C. **Ir4** or $Na_2S_2O_3$/GSH were added to normal growth media (NMG) liquid at 50°C, poured into Petri dishes (60 mm) and allowed to cool until solidified. Prepared media were seeded with the normal food source of *E. coli* and incubated overnight at room temperature to dry. Adult *C. elegans* animals were added to the $Na_2S_2O_3$/GSH loaded media and allowed to feed freely overnight. They were then fed with **Ir4** loaded media prior to imaging. Animals were transferred and imaged on 10% agarose pads in the presence of 2.5% (w/v) polystyrene beads (50 nm) to prevent movement. Imaging employed on a

monochromatic Cool SNAP FX camera (Roper Scientific, USA) and analyzed by using Axio Vision 4.2 software (Carl Zeiss).

2.8. Two-photon imaging of rat hippocampal slices

Slices were prepared from the hippocampi of 2-week-old rat (male). Coronal slices were cut into 300-400 μm thick using a vibrating blade microtome in artificial cerebrospinal fluid (ACSF: 124 mM NaCl, 3.0 mM KCl, 26.0 mM $NaHCO_3$, 1.26 mM NaH_3PO_4, 10.0 mM D-glucose, 2.5 mM $CaCl_2$ and 1.3 mM MgSO4). Slices were incubated with 2.0 μM of a **Ir4** solution in ACSF bubbled with 95% O_2/5% CO_2 for 30 min at 37 °C. Slices were then washed for times with ACSF and transferred to glass bottomed dishes and observed on a Leica TCS SP5 II MP confocal microscope. To assess the effect of sulfite movement, the slices were washed with PBS three times and pre-treated with 10 mM $BaCl_2$ for 10 min and then treated with **Ir4**. The excitation wavelength of the laser was set as 750 nm.

2.9 Tissue homogenates assays

Calibration curve of **Ir4** emission intensity at 532 nm *vs* sulfite concentration was set in PBS buffer containing 10% DMSO. Mouse tissue homogenates were obtained according to literature [37]. A two-week-old mouse was anaesthetized by intraperitoneal injection with 1% pentobarbital sodium 60 mg/kg. After transcardial perfusion with saline solution, the tissues from brain, spleen, lung, heart, kidney, serum, muscle, liver, colon and testicle were dissected out. The tissues were then homogenized in PBS buffer by a homogenizer (10^4 rpm for 10 min) on ice bath. The homogenates were centrifuged (1.3×10^4 rpm for 15 min) at 4 °C. The supernatant was taken and the concentration of protein in the homogenate was measured using a Nanodrop spectrophotometer. Homogenate was diluted to 10 mg/mL and incubated with a **Ir4** solution (5.0 μM) in PBS

containing 10% DMSO for 10 min. The emission intensity at 532 nm was recorded and sulfite content was calculated *via* calibration curve.

3. Results and discussions

3.1. Comparison of Ir(III) complexes

As a first step to identify a promising probe for *in vivo* applications, we assessed the reactivity of **Ir2**-**Ir4** with sulfite and bisulfite. Probes **Ir2**-**Ir4** were weakly emissive in PBS buffer containing 2% DMSO. When sulfite sources were added, however, the phosphorescence intensities of **Ir2**-**Ir4** increased significantly (Fig. 1b, ESI, Fig. S4-6†) by approximately 25-, 8- and 18-fold for **Ir2**, **Ir3** and **Ir4**, respectively. More importantly, these probes exhibited high selectivity toward sulfite/bisulfite over other bio-related ions and molecules (Fig. 2a). These results demonstrate the potential of **Ir2**-**Ir4** as turn-on phosphorescent probes for sulfite/bisulfite in aqueous solutions.

The phosphorescent quantum yields (ϕ) of **Ir2**-**Ir4** in the absence or presence of sulfite were calculated and listed in Table S1 (ESI). **Ir2** and **Ir3** exhibited ϕ values of 0.082 and 0.067, respectively, after reacting with sulfite, whereas **Ir4** was more efficient, with a quantum yield of 0.28 in PBS buffer. The TPA cross-section values of probes **Ir2**-**Ir4** were also determined using two-photon excitation fluorescence using rhodamine B as a standard [34,38]. As shown in Fig. 1c, probes **Ir2**-**Ir4** exhibited maximum TPA cross-section values when excited at 750 nm. The TPA cross-section values of σ_{750nm} were 36.4 GM for **Ir2**, 100.7 GM for **Ir3** and 141.0 GM for **Ir4**, and the two-photon brightness values (σ') were 2.98 GM for **Ir2**, 8.16 GM for **Ir3** and 39.5 GM for **Ir4** (ESI, Fig. S9†). The high σ' value of **Ir4** was a consequence of its high phosphorescent quantum yield and large TPA cross-section value.

In order to assess if **Ir2**-**Ir4** could be used in living cells, their cytotoxicities toward the liver cancer cell line HepG2 were also evaluated using the MTT

assay (Table 1). **Ir2** exhibited relatively moderate toxic effects over 48 h while **Ir4** was more toxic with an IC_{50} of 19.6 μM. However, when a shorter incubation time was employed (2 h), the toxicity of **Ir4** was relatively low, as evidenced by a cell viability of > 90% (ESI, Fig. S10†). On the contrary, **Ir3** was generally too toxic to be used as an *in vitro*/*in vivo* probe. Its toxicity against HepG2 cells was higher than the well-known anticancer drug cisplatin. All in all, of the three Ir(III) complexes, **Ir4** had the highest potential in TPM imaging of biological sulfite and bisulfite in living cells and tissues due to its high two-photon brightness value and relative low cytotoxicity. Thus, we utilized **Ir4** for OPM and TPM imaging and detection of biological sulfite/bisulfite in the next steps of this study.

*3.2. Sulfite sensing behaviors of **Ir4***

We first analyzed the spectral response of **Ir4** toward sulfite. When **Ir4** treated with sulfite (0-30.0 μM), its emission intensity increased linearly and then reached a plateau (Fig. 2b). As shown in Fig. 2c, the phosphorescence intensity increased rapidly, and reached a plateau within 3 min, indicating that the reaction between **Ir4** and sulfite was very fast and completed within 3 min. Job's Plot results indicated a 1:1 ratio of probe to sulfite (ESI, Fig. S7†). Of high interest, the phosphorescence intensity was barely affected when pH values were varied from 4 to 10 (ESI, Fig. S8†). Importantly, **Ir4** could also detect sulfite that was generated enzymatically *in vitro*. Indeed, when thiosulfate sulfurtransferase (TST), one of the two mitochondrial isoenzymes of rhodanese that transfers sulfur from thiosulfate to a thiophilic acceptor (CN^- or reduced glutathione (GSH)) to form sulfite or bisulfite *in vivo* [1, 39-41], was incubated with thiosulfate, GSH and **Ir4** for 10 min at 37 °C, the phosphorescence intensity increased distinctly (Fig. 2d). By contrast, no notable enhancement of emission intensity was observed when TST was absent. In addition, when TST was pre-treated with the inhibitor 2,4,6-trinitrobenzene

sulfonate (TNBS), the phosphorescence intensity sharply decreased. The reaction mechanism was evaluated using diverse analytical methods (ESI, Fig. S11-13†). Structural characterization indicated that **Ir4** reacts with sulfite through sulfite addition to the azo bond, as detailed in our previous work [27].

3.3. Intracellular sulfite imaging

Some cationic cytometalated Ir(III) complexes are known to target mitochondria [42,43]. To assess if a similar behavior was observed with **Ir4**, we used ICP-MS to investigate the subcellular localization of **Ir4**. More specifically, **Ir4** was incubated with cells for 30 min, followed by isolation of the mitochondria, nucleus and cytoplasm. ICP-MS analysis of the iridium content of these fractions (ESI, Fig. S14†) revealed that nearly 80% of **Ir4** was localized in the mitochondria (26 of 33 fg/cell), whereas only 5% of **Ir4** entered the cell nucleus (1.7 of 33 fg/cell). This result suggested that **Ir4** successfully accumulated in the mitochondria and thus could be utilized as a phosphorescent turn-on probe for biological sulfite/bisulfite in mitochondria. In addition, to further confirm the results obtained by ICP-MS, a colocalization assay using the commercial mitochondrial dye MitoTracker Red FM (MTR) was performed (Fig. 3a). The co-staining images revealed that the phosphorescence of **Ir4** overlapped well with the MTR fluorescence (overlap coefficient is 0.87), implying a preferential distribution of **Ir4** in mitochondria in agreement with our ICP-MS results.

Intracellular sulfite/bisulfite was then imaged with **Ir4** in HepG2 cells using OPM and TPM. As shown in Fig. S15a†, HepG2 cells that were incubated with 2.0 μM **Ir4** alone exhibited a faint phosphorescent signal. When cells were pre-treated with 20.0 μM sulfite for 2 h before **Ir4** incubation, however, a significant increase in the phosphorescence signal upon one-photon excitation (405 nm) was observed. A strong phosphorescence signal was also observed upon two-photon excitation (750 nm) (Fig. 3a).

As an important link in the biological sulfur cycle in the body, sulfite or bisulfite can be generated endogenously as a result of the normal metabolism of sulfur-containing amino acids. One of the most direct pathways to generate sulfite is through sulfur transfer from thiosulfate *via* catalysis by TST [39-41], which is widely distributed in nature and is particularly abundant in mammalian livers. HepG2 cells were incubated with the TST substrates $Na_2S_2O_3$/NaCN or $Na_2S_2O_3$/GSH overnight to increase cellular sulfite/bisulfite levels and were then treated with **Ir4** for 0.5 h (Fig. 3b). Remarkable phosphorescence signals were detected by TPM. In contrast, cells that were treated with GSH, $Na_2S_2O_3$ or NaCN alone in the presence of **Ir4** did not produce a detectable phosphorescent signal (ESI, Fig. S15†). In addition, when TST was deactivated by TNBS [41], very weak phosphorescence intensity was observed in the cells, suggesting that TNBS blocked sulfite/bisulfite biogeneration catalyzed by TST.

In addition, neutrophils can produce sulfite as a mediator of inflammation in response to lipopolysaccharide (LPS) stimulation, which is a major component of bacterial endotoxin [3,5]. Immune suppressive agents such as prednisolone suppress this sulfite production. However, sulfite production by neutrophils likely occurs through a sulfate-reducing pathway since sulfate can promote sulfite production. We thus stimulated mouse macrophage RAW264.7 cells with LPS and utilized **Ir4** to image sulfite production. As shown in Fig. 3c, a significant increase in phosphorescence was observed when cells were incubated with LPS. Furthermore, the addition of Na_2SO_4 to the media induced a slight enhancement (120%) in phosphorescence intensity, whereas the addition of prednisolone completely suppressed the phosphorescence intensity (32%).

3.4. In vivo sulfite imaging

With the OPM and TPM cellular imaging results in hand, we sought to expand the scope and utility of this new probe by applying it to *in vivo* imaging

of sulfite/bisulfite generated *in situ* in the model organism *C. elegans*. Many enzymes related to endogenous sulfite generation, such as rhodanese and aspartate aminotransferase (AAT), are expressed in *C. elegans* [3]. We focused our attention on the *in vivo* production of sulfite by the rhodanese/$Na_2S_2O_3$/GSH enzymatic system. *C. elegans* treated with **Ir4** alone exhibited faint phosphorescence *in vivo* as detected by TPM (Fig. 4a). However, when $Na_2S_2O_3$/GSH were included, the phosphorescence signal increased markedly and rapidly (Fig. 4b). In real-time imaging (Fig. 4c-h), some new phosphorescent spots appeared over time, indicating that endogenous sulfite was being generated *in situ* and visualized by **Ir4** in these regions.

We further investigated the utility of the probe **Ir4** in deep-tissue imaging. Fresh slices of 14-day-old rat hippocampal tissue were incubated with 2 μM of **Ir4** for 1 h at 37 °C and captured using TPM. As shown in Fig. 5a, TPM images of the slices revealed that sulfite/bisulfite were relatively evenly distributed in the CA1, CA3 and dentate gyrus (DG) regions. Moreover, images at a higher magnification clearly revealed the distribution in the individual cells in the CA1 region at a depth of 100 μm (Fig. 5b). The TPM images at depths of 80, 100, 120, 140 and 160 μm showed the sulfite/bisulfite distribution in each *xy* plane along the *z* direction (Fig. 5d). When the tissue was pre-treated with $BaCl_2$ to precipitate sulfite and bisulfite, the two-photon excited phosphorescence intensity decreased sharply (Fig. 5c). These findings demonstrate that probe **Ir4** can effectively enable the determination of sulfite/bisulfite levels at depths of 80-160 μm in live tissues using TPM.

Importantly, the rat hippocampal slices were not pre-treated with any sulfite sources (exogenous or endogenous), and the TPM images demonstrated the distribution of sulfite/bisulfite in rat brain. This may be the first visual evidence of SO_2 derivatives in a rat brain. To confirm the results of *in vivo* images, we further detected sulfite/bisulfite contents using tissue homogenates assays. Brain tissue as well as spleen, lung, heart, kidney, liver, serum, muscle, colon and testicle were separated from rats and homogenized immediately as

described by Zhao, Xu and co-workers in previous work [37,44]. A calibration curve was constructed with sulfite concentrations ranging from 1.0 μM to 20.0 μM (R = 0.9988) (Fig. 6a). The average sulfite concentration in serum was 10.20 ± 1.21 μM. This result is in good agreement with other reports, which used HPLC methods [45,46]. The average sulfite concentration in the brain tissues of 3 rats was 8.39 ± 0.80 μM (Fig. 6b). In addition, sulfite was abundant in colon and muscle tissues and less distributed in spleen and lung, most likely due to its biological functions as an antioxidant and in vascular smoothing [3]. These values are likely an overestimate because the high concentration of reduced biothiols such as GSH *in vivo* would increase the response to **Ir4** and, consequently, the phosphorescence intensity (see Fig. 2a). Importantly, these observations are in agreement with the *in vivo* images of this study.

4. Conclusion

In recent years, an increasing amount of research has focused on the biological effects of endogenous SO_2 and its derivatives (sulfite/bisulfite) and revealed their physiological importance in cardiovascular system [1-10]. However, *in vivo* detection of sulfite/bisulfite remains challenging. In this study we sought to develop an efficient two-photon probe for real-time imaging of SO_2 derivatives *in vivo*. A series of dinuclear Ir(III) complexes (**Ir2**-**Ir4**) bearing an azo group as the sulfite-active moiety were synthesized, and their sulfite sensing behaviors, photophysical properties and cytotoxicities towards cancer cells compared. These Ir(III) complexes could rapidly react with sulfite resulting in an increase in phosphorescence intensity. **Ir4** was found to have the greatest quantum yield of the series of organometallic complexes (ϕ (**Ir4**) = 0.28 compared to ϕ (**Ir2**) = 0.082 and ϕ (**Ir3**) = 0.081). In addition, **Ir4** exhibited a large value of TPA cross-section, resulting in a large two-photon brightness value (σ' = 39.5), while σ' (**Ir2**) = 2.98 and σ' (**Ir3**) = 8.16. Importantly, **Ir4** showed relative low cytotoxicity against HepG2 cells. Indeed,

after 2 h incubation time, the toxicity of **Ir4** was relatively low, as evidenced by a cell viability of > 90%, suggesting that, in our experimental conditions (2.0 μM for 0.5 h incubation), **Ir4** was nearly non-toxic. All in all, due to these favorable properties (i.e. large two-photon brightness value and relative low cytotoxicity), **Ir4** was chosen as the lead compound for further studies. We therefore then assessed its potential for OPM and TPM imaging and detection of biological sulfite/bisulfite.

Ir4 was found to be an Off-On phosphorescent probe for sulfite and bisulfite with high sensitivity, selectivity and rapid response. As required for biological applications, this probe preferentially targeted mitochondria and, importantly, enabled the direct visualization of intracellular sulfite/bisulfite levels using OPM and TPM. **Ir4** allowed for the imaging of endogenous sulfite/bisulfate within living cells, and this using different sulfite/bisulfate generation pathways. Its application to *in vivo* imaging was then investigated in the model organism *C. elegans* by TPM. Real-time imaging of *C. elegans* using **Ir4** allows for the visualization of sulfite/bisulfite generation *in situ*. Even more strikingly, *in vivo* deep-tissue imaging was expanded to fresh slices of rat hippocampal tissue using TPM. The images suggested that sulfite is distributed in the brain with a concentration of 8.39 ± 0.80 μM. All in all, our findings demonstrate that the probe **Ir4** is a useful and convenient tool for the detection and imaging of biological sulfite/bisulfite in subcellular organelles or live tissues using TPM. The successful visualization of SO_2 derivatives in rat brains is of particular significance since the potential role of SO_2 as a gasotransmitter remains unclear. We hope that our findings will facilitate the elucidation of the biological functions of SO_2.

Funding

This work was supported by the 973 program (Nos. 2014CB845604 and 2015CB856301), the National Science Foundation of China (Nos. 21172273, 21171177, and 21471164), Program for Changjiang Scholars and Innovative Research Team in University of China (No. IRT1298), the Swiss National Science Foundation (SNSF Professorships PP00P2_133568 and PP00P2_157545 to G.G.) and the University of Zurich.

Appendix A. Supplementary data

Supplementary data related to this article can be found at http://dx.doi.org/

Figure Captions

Fig. 1	(a) Chemical structures of **Ir1**-**Ir4**. (b) Normalized emission intensity of **Ir1**-**Ir4** after reacting with sulfite. (c) Two-photon absorption cross-section of **Ir1**-**Ir4** after reacting with sulfite.
Fig. 2	(a) Relative intensity of **Ir4** (5 μM) treated with different species (1 mM for each species except 20 μM for sulfite and bisulfite) in PBS buffer containing 2% DMSO. $\lambda_{ex/em}$ = 405 nm/532 nm. Bars: 1, Control; 2, NaCl; 3, NaI; 4, Na_2CO_3; 5, $NaNO_2$; 6, $NaNO_3$; 7, Na_2SO_4; 8, NaCN; 9, citrate; 10, EDTA; 11, boric acid; 12, H_2O_2; 13, TEMPO; 14, Na_2S; 15, $Na_2S_2O_3$; 16, Cys; 17, Hcy; 18, GSH; 19, Asc; 20, DTT; 21, Na_2SO_3; 22, $NaHSO_3$. (b) Emission spectra of **Ir4** (5 μM) with increasing sulfite concentration. Insert: relative intensity at 532 nm *vs* sulfite concentration. (c) Time-dependent curves of **Ir4** (5 μM) emission intensity with 20 μM sulfite solution in PBS containing 2% DMSO. (d) Enzymatic generation of sulfite or bisulfite by TST. A solution of GSH/$Na_2S_2O_3$ or NaCN/$Na_2S_2O_3$ (20 mM/10 mM) was incubated with a 5 μM **Ir4** solution in PBS buffer containing 0.3% DMSO at 37 °C. Human TST-6* His fusio protein (15 μg •L^{-1}) was then added to the mixture and incubated for 10 min 37°C. TNBS was added to inhibit TST activity. $\lambda_{ex/em}$ = 405/532 nm. Slits were set to 10 nm.
Fig. 3	Confocal fluorescent images of **Ir4** (2.0 μM) indicating intracellular sulfite/bisulfite. (a) Using **Ir4** to image exogenous sulfite. From left to right: OPM of Cells that were pre-treated with sulfite (20 μM) for 2 h and then **Ir4** for 0.5 h; TPM of Cells that were pre-treated with sulfite and then **Ir4**; Co-stained with Mito Tracker Red (MTR); Overlay of TPM image and MTR image. (b) Two-photon images of endogenous sulfite/bisulfite that generated *via* rhodanase catalysis. HepG2 cells were pre-treated with 500 μM/250 μM TST

	substrates $Na_2S_2O_3$/NaCN or $Na_2S_2O_3$/GSH overnight to increase sulfite/bisulfite levels, followed by treatment with **Ir4** for 0.5 h min. As a negative control, TST activity was inhibited by 100 mM TNBS. (c) Two-photon images of endogenous sulfite/bisulfite that generated *via* LPS stimulation. LPS (1 μg/mL) was added to stimulate RAW264.7 cells for 2 h. Sulfate (100 μM) was treated with RAW264.7 cells for 4 h after LPS treatment to promote sulfite production. And 0.1 μM prednisolone was added to incubate for 4 h before LPS treatment to suppress sulfite production. Luminescent signal collection ($\lambda_{ex/em}$): OPM 405/550±30 nm and TPM 750/550±30 nm for **Ir4**; 543/630±30 nm for MTR. Scale bars in (a-l): 20 μm.
Fig. 4	TPM images of *C. elegans* loaded with **Ir4** (2.0 μM). (a) *C. elegans* treated with **Ir4** at 20 °C for 30 min. (b) *C. elegans* pre-treated overnight with 500 μM/250 μM of $Na_2S_2O_3$/GSH and then treated with **Ir4** at 20 °C. (c–h) Real-time TPM images of (b). The arrows indicate *in situ* generation of endogenous sulfite in *C. elegans*. Scale bars: 20 μm.
Fig. 5	TPM image of a fresh rat hippocampal slice stained with **Ir4** (2.0 μM) for 1 h (a) under ×10 magnification and (b) under ×100 magnification in the CA1 region. (c) TPM image of a slice pre-treated with 10 mM $BaCl_2$ for 10 min before labelling with **Ir4**. (d) TPM images of the slice were acquired at different scanning depths (80-160 μm). Scale bars in (a), (c) and (d): 200 μm. Scale bar in (b): 25 μm.
Fig. 6	(a) Calibration curve of phosphorescence intensity vs. sulfite concentration in PBS buffer containing 10% DMSO. Tissue homogenates were incubated with **Ir4** (5.0 μM) at 37 °C for 5 min, and the emission intensity was then recorded. (b) Sulfite

	concentrations in different tissue homogenates were calculated *via* calibration curve (a). All homogenate concentrations were standardized to 10 mg/mL.

References

[1] Ji AJ, Savon SR, Jacobsen DW. Determination of total serum sulfite by HPLC with fluorescence detection. Clin Chem 1995; 41: 897–903.

[2] Mathew ND, Schlipalius DI, Ebert PR. Sulfurous gases as biological messengers and toxins: comparative genetics of their metabolism in model organisms. J Toxicol 2011; 2011:394970.

[3] Tsuzuki T, Obaru K, Setoyama C, Shimada K. Structural organization of the mouse mitochondrial aspartate aminotransferase gene. J Mol Biol 1987;198:21-31.

[4] Mitsuhashi H, Yamashita S, Ikeuchi H, Kuroiwa T, Kanelo Y, Hiromura K, Ueki K, Nojima Y. Oxidative stress-dependent conversion of hydrogen sulfide to sulfite by activated neutrophils. Shock 2005;24:229–34.

[5] Mitsuhashi H, Nojima Y, Tanaka T, Ueki K, Maezawa A, Yano S, Naruse T. Sulfite is released by human neutrophils in response to stimulation with lipopolysaccharide. J Leukocyte Biol 1998;64:595-9.

[6] Wang XB, Jin HF, Tang CS, Du JB. The biological effect of endogenous sulfur dioxide in the cardiovascular system. Eur J Pharmacol 2011; 670:1-6.

[7] Wang XB, Jin HF, Tang CS, Du JB. Significance of endogenous sulphur-containing gases in the cardiovascular system. Clin Exp Pharmacol Physiol 2010;37:745-52.

[8] Meng Z, Zhang H. The vasodilator effect and its mechanism of sulfur dioxide-derivatives on isolated aortic rings of rats. Inhal Toxicol 2007;19: 979-86.

[9] Hart JL. Role of sulfur-containing gaseous substances in the cardiovascular system. Front Biosci 2011;3:736-49.

[10] Li X, Bazer FW, Gao H, Jobgen W, Johnson GA, Li P, McKnight JR, Satterfield MC, Spencer TE, Wu G. Amino acids and gaseous signaling. Amino Acids 2009;37:65-78.

[11] Yang YM, Zhao Q, Feng W, Li FY. Luminescent chemodosimeters for bioimaging. Chem Rev 2013;113:192-270.

[12] Ma D, Ma VP, Chan DS, Leung K, He H, Leung C. Recent advances in luminescent heavy metal complexes for sensing. Coord Chem Rev 2012;256:3087-113.

[13] You Y. Phosphorescence bioimaging using cyclometalated Ir(III) complexes. Curr Opin Chem Biol 2013;17:699-707.

[14] Chan J, Dodani SC, Chang CJ. Reaction-based small-molecule fluorescent probes for chemoselective bioimaging. Nat Chem 2012;4:973-84.

[15] Santos-Figueroa LE, Gimenez C, Agostini A, Aznar E, Marcos MD, Sancenon F, Martinez-Manez R, Amonos P. Selective and sensitive chromofluorogenic detection of the sulfite anion in water using hydrophobic hybrid organic–inorganic silica nanoparticles. Angew Chem Int Ed 2013;125:13957-61.

[16] Sun Y, Zhao D, Fan S, Duan L, Li R. Ratiometric fluorescent probe for rapid detection of bisulfite through 1,4-addition reaction in aqueous solution. J Agric Food Chem 2014;62:3405-9.

[17] Wu M, He T, Li K, Wu M, Huang Z, Yu X. A real-time colorimetric and ratiometric fluorescent probe for sulfite. Analyst 2013;138:3018-25.

[18] Tian H, Qian J, Sun Q, Bai H, Zhang W. Colormetric and ratiometric fluorescent detection of sulfite in water via cationic surfant-promoted addition of sulfite to α,β-unsaturated ketone. Anal Chim Acta 2013;788:165-70.

[19] Wu M, Li K, Li C, Hou J, Yu X. A water-soluble near-infrared probe for colormetric and ratiometric sensing of SO_2 derivatives in living cells. Chem Commun 2014;50:183-5.

[20] Peng M, Yang X, Yin B, Guo Y, Suzent F, En D, Li J, Li C, Duan Y. A hybrid coumarin-thizaole fluorescent sensor for selective detection of bisulfite anions in vivo and in real samples. Chem Asian J 2014;9:1817-22.

[21] Sun Y, Liu J, Zhang J, Yang T, Guo W. Fluorescent probe for biological gas SO_2 derivatives bisulfite and sulfite. Chem Commun 2013;49:2637-9.

[22] Zipfel WR, Williams RM, Webb WW. Nonlinear magic: multiphoton microscopy in the biosciences. Nat Biotechnol 2003;21:1369-77.

[23] Helmchen F, Denk W. Deep tissue two-photon microscopy. Nat Methods 2005;2:932-40.

[24] Drobizhev M, Makarov NS, Tillo SE, Hughes TE, Rebane A. Two-photon absorption properties of fluorescent proteins. Nat Methods 2011;8:393-9.

[25] Kim HM, Cho BR. Two-photon probes for intracellular free metal ions, acidic vesicles, and lipid rafts in live tissues. Accounts Chem Res 2009;42:863-72.

[26] Bort G, Gallavardin T, Ogden D. Dalko PI. From one-photon to two-photon probes: "caged" compounds, actuators, and photoswitches. Angew Chem Int Ed 2013;52:4526-37.

[27] Li G, Chen Y, Wang J, Lin Q, Zhao J, Ji L, Chao H. A dinuclear iridium(III) complex as a visual specific phosphorescent probe for endogenous sulphite and bisulphite in living cells. Chem Sci 2013;4:4426-33.

[28] Kim HJ, Heo CH, Kim HM. Benzimidazole-Based Ratiometric Two-Photon Fluorescent Probes for Acidic pH in Live Cells and Tissues. J Am Chem Soc 2013;135:17969-17977.

[29] Bae SK, Heo CH, Choi DJ, Sen D, Joe E, Cho BR, Kim HM. A Ratiometric Two-Photon Fluorescent Probe Reveals Reduction in Mitochondrial H_2S Production in Parkinson's Disease Gene Knockout Astrocytes. J Am Chem Soc 2013;135:9915-9923.

[30] Xu H, Yu D, Liu L, Yan P, Jia L, Li G, Yue Z. Small molecular glasses based on multiposition encapsulated phenyl benzimidazole iridium(III) complexes: toward efficient solution-processable host-free electrophosphorescent diodes. J Phys Chem B 2010;114:141–50.

[31] Cho YH, Lee CY, Cheon CH. Cyanide as a powerful catalyst for facile synthesis of benzofused heteroaromatic compounds via aerobic oxidation. Tetrahedron 2013;69:6565-73.

[32] Li G, Chen Y, Wu J, Ji L, Chao H. Thiol-specific phosphorescent imaging in living cells with an azobis(2,2'-bipyridine)-bridged dinuclear iridium(III) complex. Chem Commun 2013;49:2040-2.

[33] Caspar JV, Meyer TJ. Photochemistry of tris(2,2'-bipyridine) ruthenium(2+) ion ($Ru(bpy)_3^{2+}$). Solvent effects. J Am Chem Soc 1983;105:5583-90.

[34] Xu C, Webb WW. Measurement of two-photon excitation cross sections of molecular fluorophores with data from 690 to 1050 nm. J Opt Soc Am B 1996;13: 481-91.

[35] Makarov NS, Drobizhev M, Rebane A. Two-photon absorption standards in the 550–1600 nm excitation wavelength range. Opt Express 2008;16:4029-47.

[36] Brenner S. The genetics of Caenorhabditis elegans. Genetics 1974;77:71-94.

[37] Wang X, Cui L, Zhou N, Zhu W, Wang R, Qian X, Xu Y. A highly selective and sensitive near-infrared fluorescence probe for arylamine N-acetyltransferase 2 in vitro and in vivo. Chem Sci 2013:4:2936-40.

[38] Albota MA, Xu C, Webb WW. Two-photon fluorescence excitation cross sections of biomolecular probes from 690 to 960 nm. Appl Opt 1998;37:7352-6.

[39] Ploegman JH, Drent G, Kalk KH, Hol WGJ. The covalent and tertiary structure of bovine liver rhodanese. Nature 1978;273:124-9.

[40] Cipollone R, Ascenzi P, Tomao P, Imperi F, Visca P. Enzymatic detoxification of cyanide: clues from Pseudomonas aeruginosa Rhodanese. J Mol Microbiol Biotechnol 2008;15:199–211.

[41] Malliopoulou VA, Rakitzis ET, Malliopoulou TB. Inactivation of rhodanese from human gastric mucosa and stomach adenocarcinoma by 2,4, 6-trinitrobenzenesulphonate and by 4,4'-diisothiocyanatostilbene-2,2'- sulphonate. Anticancer Res 1989;9:1133-6.

[42] Chen Y, Qiao L, Yu B, Li G, Liu C, Ji L, Chao H. Mitochondria-specific phosphorescent imaging and tracking in living cells with an AIPE-active iridium(III) complex. Chem Commun 2013;49:11095-7.

[43] Chen Y, Qiao L, Ji L, Chao H. Phosphorescent iridium(III) complexes as multicolor probes for specific mitochondrial imaging and tracking. Biomaterials 2014;35:2-13.

[44] Qian Y, Zhang L, Ding S, Deng X, He C, Zheng XE, Zhu H, Zhao J. A fluorescent probe for rapid detection of hydrogen sulfide in blood plasma and brain tissues in mice. Chem Sci 2012;3:2920-3.

[45] Du S, Jin H, Bu D, Zhao X, Geng B, Tang C, Du J. Endogenously generated sulfur dioxide and its vasorelaxant effect in rats. Acta Pharmacol Sin. 2008; 9:923-30.

[46] Meng Z, Li J, Zhang Q, Bai W, Yang Z, Zhao Y, Wang F. Vasodilator effect of gaseous sulfur dioxide and regulation of its level by Ach in rat vascular tissues. Inhal Toxicol 2009;21:1223-8.

Table 1 Quantum yields, TPA cross-sections, TPA action cross-sections and cytotoxicities of **Ir1**-**Ir4** in the absence or presence of sulfite.

Complex	Em./nm	Lifetime/ns	Φ/%	σ/GM [a]	σ′/GM [b]	IC_{50}/μM [c]
Ir1	591	72.2	0.18	0.45	0.00081	31.5 ± 4.5
Ir1 + Sulfite	588	155.7	8.3	51.3	4.26	40.9 ± 5.1
Ir2	591	117.6	0.32	0.42	0.0013	49.2 ± 6.2
Ir2 + Sulfite	593	229.3	8.2	36.4	2.98	63.1 ± 5.6
Ir3	513, 544	151.4	0.57	1.12	0.0064	4.0 ± 1.1
Ir3 + Sulfite	514, 541	454.6	8.1	100.7	8.16	5.9 ± 1.3
Ir4	529, 570	124.8	1.5	2.37	0.036	19.6 ± 3.5
Ir4 + Sulfite	532, 567	825.7	28	141.0	39.5	23.4 ± 3.1

(a)1 GM = 10^{-50} $cm^4 \cdot s \cdot photon^{-1}$; (b) Two-photon brightness value, $\sigma' = \sigma \times \phi$; (c) Cytotoxicity against HepG2 cells for 48 h, with a reference of 12.0 ± 1.1 μM for cisplatin against HepG2 cells.

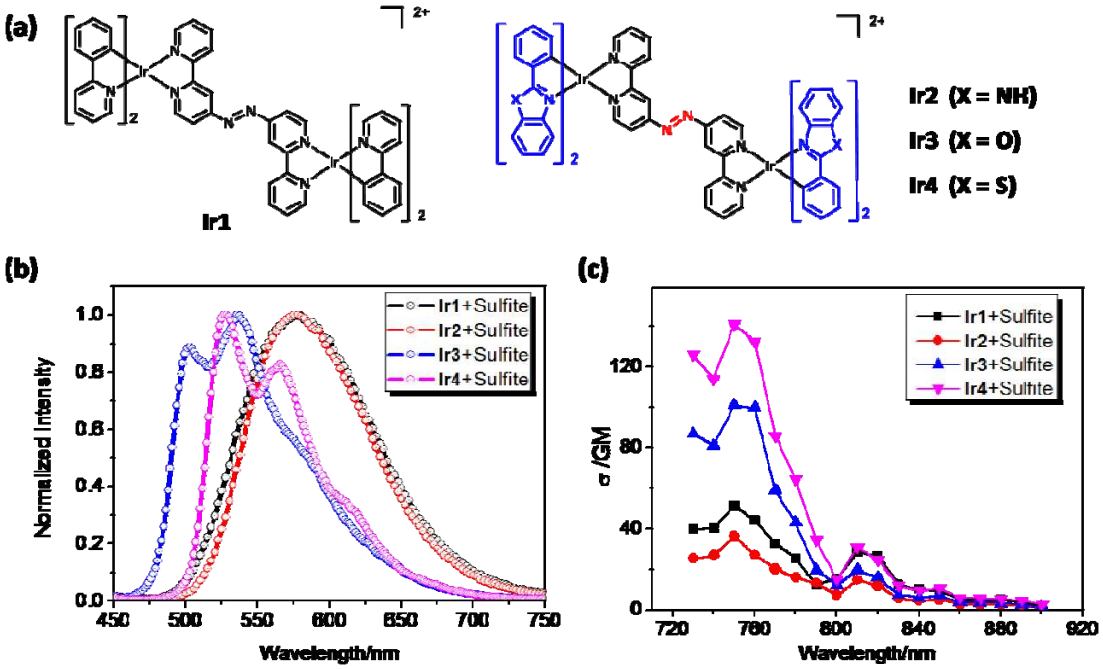

Fig. 1 (a) Chemical structures of **Ir1**-**Ir4**. (b) Normalized emission intensity of **Ir1**-**Ir4** after reacting with sulfite. (c) Two-photon absorption cross-section of **Ir1**-**Ir4** after reacting with sulfite.

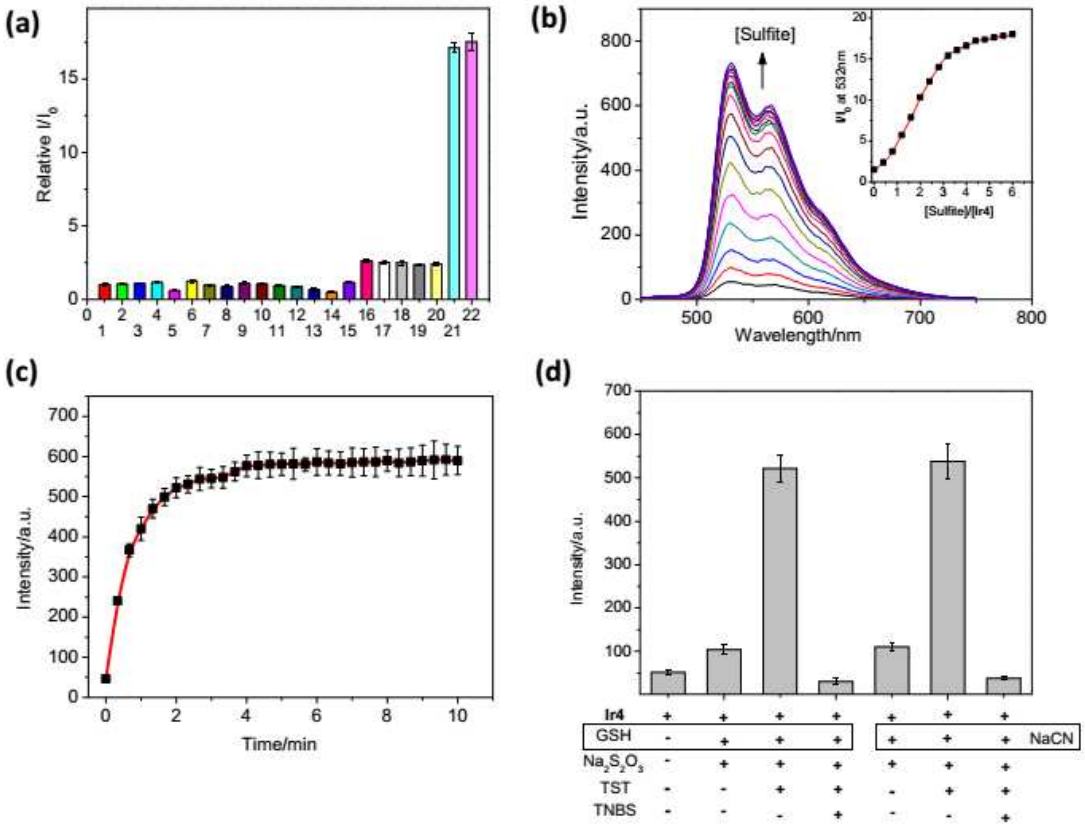

Fig. 2 (a) Relative intensity of **Ir4** (5 μM) treated with different species (1 mM for each species except 20 μM for sulfite and bisulfite) in PBS buffer containing 2% DMSO. $\lambda_{ex/em}$ = 405 nm/532 nm. Bars: 1, Control; 2, NaCl; 3, NaI; 4, Na_2CO_3; 5, $NaNO_2$; 6, $NaNO_3$; 7, Na_2SO_4; 8, NaCN; 9, citrate; 10, EDTA; 11, boric acid; 12, H_2O_2; 13, TEMPO; 14, Na_2S; 15, $Na_2S_2O_3$; 16, Cys; 17, Hcy; 18, GSH; 19, Asc; 20, DTT; 21, Na_2SO_3; 22, $NaHSO_3$. (b) Emission spectra of **Ir4** (5 μM) with increasing sulfite concentration. Insert: relative intensity at 532 nm *vs* sulfite concentration. (c) Time-dependent curves of **Ir4** (5.0 μM) emission intensity with 20 μM sulfite solution in PBS containing 2% DMSO. (d) Enzymatic generation of sulfite or bisulfite by TST. A solution of GSH/$Na_2S_2O_3$ or NaCN/$Na_2S_2O_3$ (20 mM/10mM) was incubated with a 5.0 μM **Ir4** solution in PBS buffer containing 0.3% DMSO at 37°C. Human TST-6* His fusio protein (15 μg •L^{-1}) was then added to the mixture and incubated for 10 min 37°C. TNBS was added to inhibit TST activity. $\lambda_{ex/em}$ = 405/532 nm. Slits were set to 10 nm.

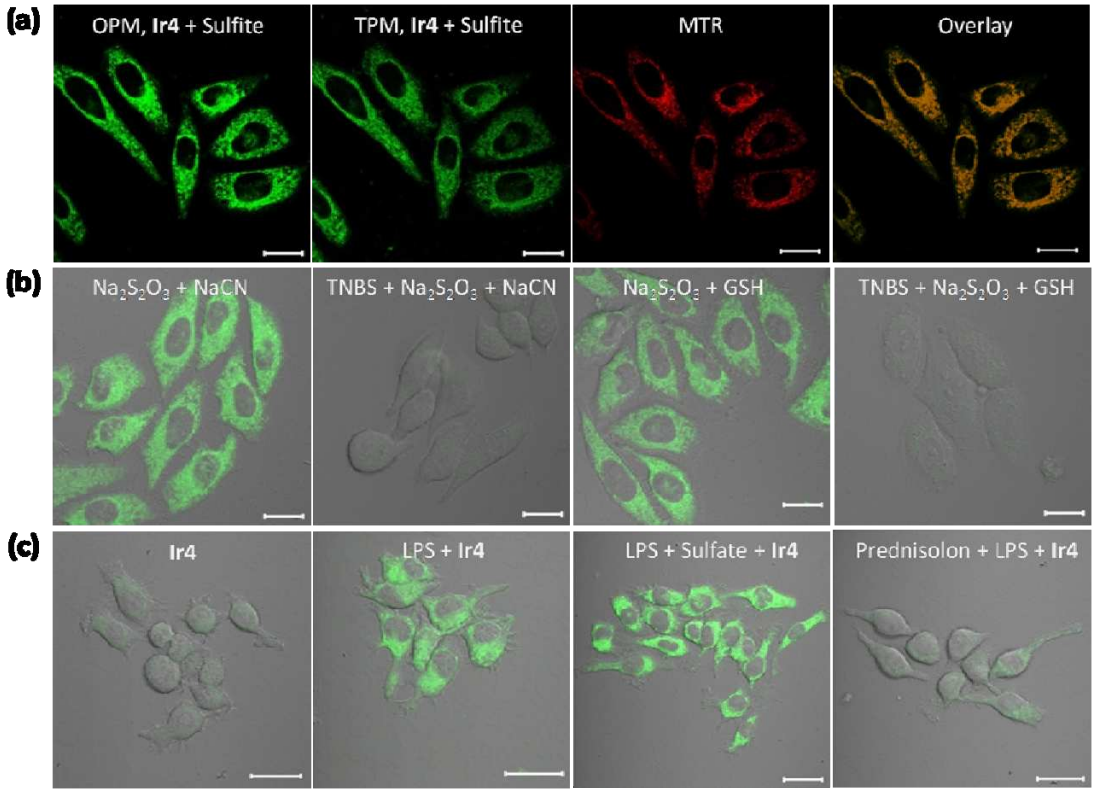

Fig. 3 Confocal fluorescent images of **Ir4** (2.0 μM) indicating intracellular sulfite/bisulfite. (a) Using **Ir4** to image exogenous sulfite. From left to right: OPM of Cells that were pre-treated with sulfite (20 μM) for 2 h and then **Ir4** for 0.5 h; TPM of Cells that were pre-treated with sulfite and then **Ir4**; Co-stained with Mito Tracker Red (MTR); Overlay of TPM image and MTR image. (b) Two-photon images of endogenous sulfite/bisulfite that generated *via* rhodanase catalysis. HepG2 cells were pre-treated with 500 μM/250 μM TST substrates $Na_2S_2O_3$/NaCN or $Na_2S_2O_3$/GSH overnight to increase sulfite/bisulfite levels, followed by treatment with **Ir4** for 0.5 h min. As a negative control, TST activity was inhibited by 100 mM TNBS. (c) Two-photon images of endogenous sulfite/bisulfite that generated *via* LPS stimulation. LPS (1 μg/mL) was added to stimulate RAW264.7 cells for 2 h. Sulfate (100 μM) was treated with RAW264.7 cells for 4 h after LPS treatment to promote sulfite production. And 0.1 μM prednisolone was added to incubate for 4 h before LPS treatment to suppress sulfite production. Luminescent signal collection ($\lambda_{ex/em}$): OPM 405/550±30 nm and TPM 750/550±30 nm for **Ir4**; 543/630±30 nm for MTR. Scale bars in (a-l): 20 μm.

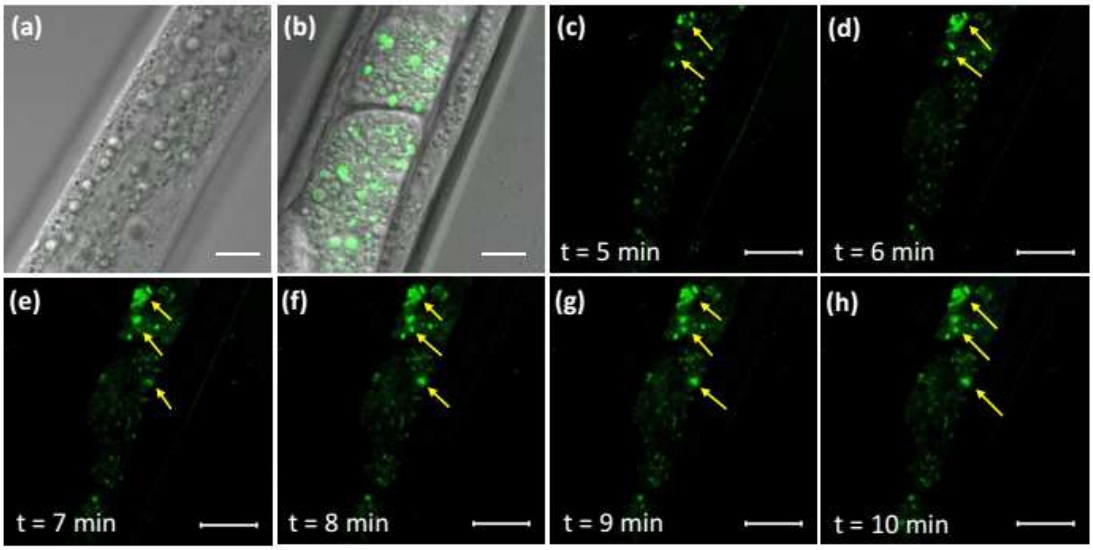

Fig. 4 TPM images of *C. elegans* loaded with **Ir4** (2.0 μM). (a) *C. elegans* treated with **Ir4** at 20 °C for 30 min. (b) *C. elegans* pre-treated overnight with 500 μM/250 μM of $Na_2S_2O_3$/GSH and then treated with **Ir4** at 20 °C. (c–h) Real-time fluorescent images of (b). The arrows indicate *in situ* generation of endogenous sulfite in *C. elegans*. Scale bars: 20 μm.

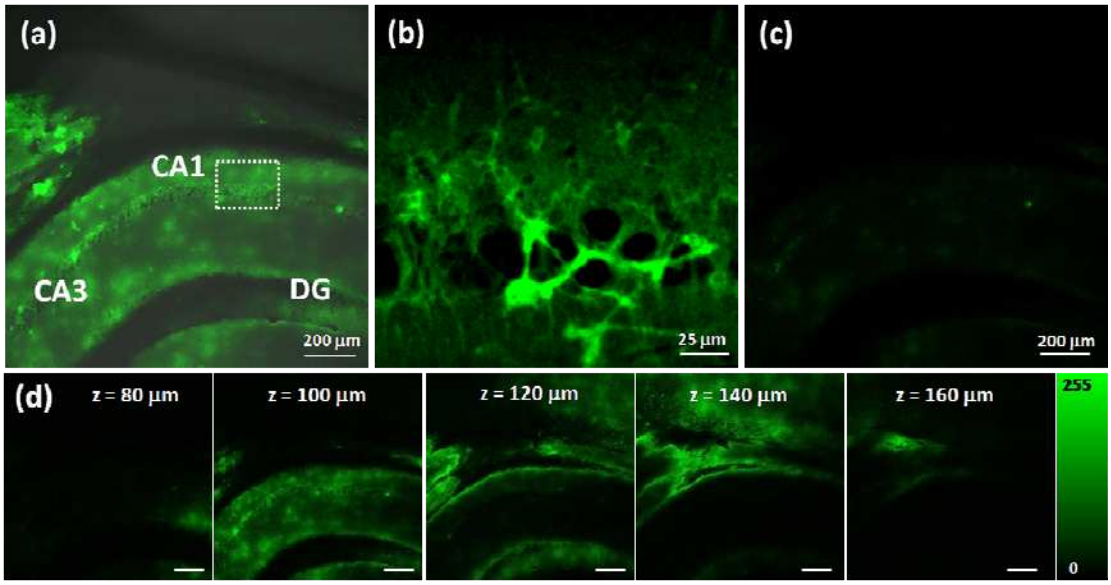

Fig. 5 TPM image of a fresh rat hippocampal slice stained with **Ir4** (2.0 μM) for 1 h (a) under ×10 magnification and (b) under ×100 magnification in the CA1 region. (c) TPM image of a slice pre-treated with 10 mM $BaCl_2$ for 10 min before labeling with **Ir4**. (d) TPM images of the slice were acquired at different scanning depths (80-160 μm). Scale bars in (a), (c) and (d): 200 μm. Scale bar in (b): 25 μm.

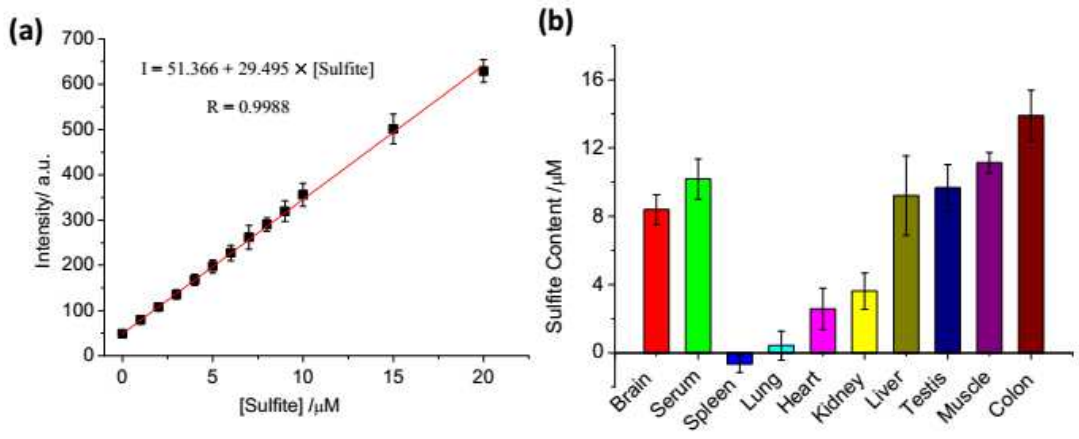

Fig. 6 (a) Calibration curve of phosphorescence intensity vs. sulfite concentration in PBS buffer containing 10% DMSO. Tissue homogenates were incubated with **Ir4** (5.0 μM) at 37 °C for 5 min, and the emission intensity was then recorded. (b) Sulfite concentrations in different tissue homogenates were calculated *via* calibration curve (a). All homogenate concentrations were standardized to 50 mg/mL.